

Nonhalogenated Solvent Processable and Printable High-Performance Polymer Semiconductor Enabled by Isomeric Nonconjugated Flexible Linkers

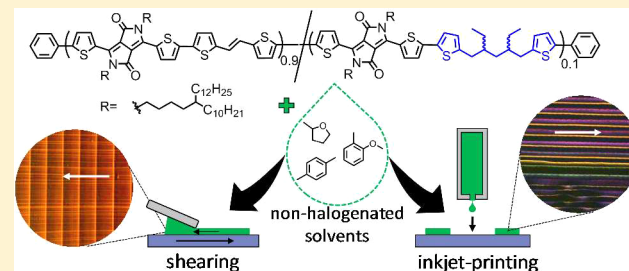
Ging-Ji Nathan Wang,^{ID} Francisco Molina-Lopez, Hongyi Zhang, Jie Xu, Hung-Chin Wu,^{ID} Jeffrey Lopez, Leo Shaw,^{ID} Jaewan Mun, QiuHong Zhang, Sihong Wang, Anatol Ehrlich, and Zhenan Bao^{*ID}

Department of Chemical Engineering, Stanford University, Stanford, California 94305-5025, United States

Supporting Information

ABSTRACT: One major advantage of organic electronics is their superior processability relative to traditional silicon-based materials. However, most high-performing polymer semiconductors exhibit poor solubility and require toxic chlorinated solvents coupled with inefficient coating methods such as spin-coating for device fabrication. Therefore, developing polymer semiconductors that are processable in environmentally benign solvents and compatible with effective printing techniques while maintaining good charge transport properties is crucial for the industrialization of low-cost and lightweight plastic electronics.

In this study, alkyl flexible linkers with branched tertiary carbon atoms are inserted to a high-mobility diketopyrrolopyrrole-based polymer backbone to suppress polymer aggregation in solution, decrease crystallinity, and increase free volume. The polymer readily dissolves in industrial solvents and shows a 70-fold increase in solubility compared to its fully conjugated counterpart. Furthermore, due to its high solubility, the polymer can be inkjet-printed and solution-sheared at high concentrations using eco-friendly solvents such as *p*-xylene and 2-methyltetrahydrofuran with a maximum hole mobility of $2.76 \text{ cm}^2 \text{ V}^{-1} \text{ s}^{-1}$ and on-off ratio above 10^5 in organic field-effect transistors.



1. INTRODUCTION

Polymer semiconductors are emerging materials for wearable and implantable electronics due to their intrinsic flexibility,^{1–4} relative low tensile modulus, and biocompatibility.^{5–7} Furthermore, organic semiconductors are often known for their high chemical tunability and processability, which can yield low-cost electronics via solution-based printing and coating techniques compatible with high-throughput roll-to-roll processes.^{8–10} The promise is that the ease of fabrication for organic electronics could one day be comparable to that of printing newspapers.¹¹ Yet current record-performing polymer semiconductors still require the spin-coating of toxic chlorinated solvents at elevated temperatures for device fabrication, which is nonideal in industrial settings.^{12–14} The removal of hazardous solvents and the utilization of efficient printing techniques are therefore vital toward the commercialization of polymer semiconductors.¹⁵

For organic photovoltaics (OPVs), significant progress has been made recently in developing green-solvent processable polymer solar cells.^{16–19} Ye et al. demonstrated blade coating of polymer:fullerene OPVs and all-polymer OPVs with high power conversion efficiencies using a benign food additive as solvent.²⁰ Similarly, Zhao et al. did so using environmentally friendly solvents such as tetrahydrofuran mixed with isopropyl alcohol.²¹ The dissolution of high-mobility polymers for organic field-effect transistors (OFETs), on the other hand,

remains a challenge due to the rigid polymer backbones, high molecular weights, and strong aggregation properties that are essential for good charge transport.^{22–25} Thermodynamically, high-performance conjugated polymers exhibit strong intermolecular interactions, causing large free volume dissimilarity between polymer and solvent molecules and the free energy change of solvation less negative.^{26,27}

One common approach to enhance polymer semiconductor processability is by introducing solubilizing side-chains.^{28–30} Matthews et al. have shown that increasing alkyl side-chain length and volume ratio could improve polymer solubility in nonhalogenated solvents such as toluene, xylenes, and tetralin.³¹ Others have incorporated ethylene glycol-based side-chains to increase polymer processability in polar solvents such as tetrahydrofuran, ethanol, and even water.^{32–35} Low field-effect hole mobilities ($\mu_h < 10^{-2} \text{ cm}^2 \text{ V}^{-1} \text{ s}^{-1}$) were, however, achieved for water/alcohol processed devices. Another strategy is to introduce backbone asymmetry to disrupt molecular aggregation in solution, which could be done through random copolymerization³⁶ or the incorporation of asymmetric monomer units^{37,38} to weaken $\pi-\pi$ interactions. However, these studies still use spin-coating as their film

Received: May 6, 2018

Revised: June 7, 2018

Published: June 25, 2018

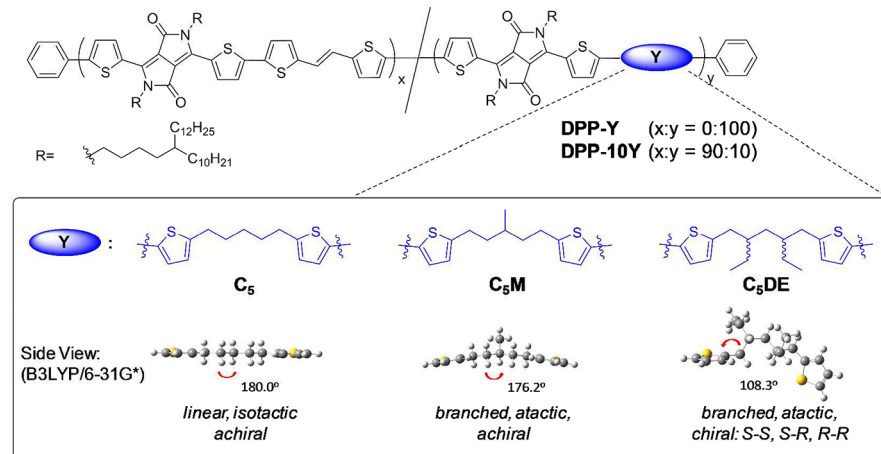


Figure 1. Schematic showing the chemical structure of the DPP-based polymers used in this study and their respective C_5 flexible linkers. Side views of the flexible linker monomers' optimized molecular conformation were calculated by density functional theory (DFT). The S–R isomer of C_5 DE is shown; the S–S or R–R isomers' molecular conformation could be found in the Supporting Information (Figure S6).

Table 1. Molecular Weight and Physical Properties of the Different Nonconjugated DPP Polymers

polymer	x:y ^a	M_n (kg mol ⁻¹) ^b	M_w (kg mol ⁻¹) ^c	D_w ^d	DP _n ^e	T_g^1 (°C) ^f	T_g^2 (°C) ^g	T_m (°C) ^h	ΔH_{fus} (J g ⁻¹) ⁱ
DPP- C_5	0:100	18.7	28.4	1.52	14.5	-49.2		148.7	13.6
DPP- C_5 M	0:100	22.2	31.1	1.40	17.0	-48.7		117.9	7.6
DPP- C_5 DE	0:100	13.6	26.1	1.92	10.1	-53.8	5.6	56.6	0.7

^a1,2-(E)-Bis(5'-trimethylstannanyl-2'-C-thienyl)ethene (TVT):flexible linker monomer ratio. ^bNumber-average molecular weight. ^cWeight-average molecular weight. ^dWeight dispersity, defined as M_w/M_n . ^eDegree of polymerization. ^fSide-chain glass transition temperature measured by differential scanning calorimetry. ^gBackbone glass transition temperature measured by differential scanning calorimetry. ^hMelting temperature. ⁱMelting temperature.

deposition method, which is not scalable for large area deposition and a wasteful process—as the majority of polymer ink is spun off the substrate. The implementation of large area coating techniques such as slot-die-coating, gravure-coating, and blade-coating using benign solvents, on the other hand, is nontrivial as well-dissolved and highly stable polymer inks (concentrations >10 mg mL⁻¹) are often desired,¹⁵ whereas spin-coating could be performed with concentrations as low as 2 mg mL⁻¹. Other patterning techniques such as inkjet printing require well-dissolved inks that could be filtered through a submicrometer filter to prevent the clogging of the inkjet nozzle.

Here, we design a highly processable diketopyrrolopyrrole (DPP)-based polymer with isomeric flexible linkers that could be solution-sheared and inkjet-printed using nonhalogenated solvents for high-performance OFETs. Recently, several groups reported the use of nonconjugated flexible linkers to enhance the processability,^{39,40} stability,^{41–43} and stretchability^{44,45} of polymer semiconductors with minimal compromise in device performance. Zhao et al. further demonstrated that the addition of linear alkyl linkers could greatly lower the melting temperature (T_m) of polymer semiconductors, allowing them to be melt-processed at high temperatures (>100 °C).^{46–48} To date, all studies have focused on isotactic, linear secondary carbon linkers with varied molar percentages and alkyl lengths. In this paper, we investigate for the first time the effect of atactic, branched tertiary carbon atoms in the flexible linkers on the semiconductor's optoelectronic properties and solution processability. We hypothesize that the insertion of branched flexible linkers can be an effective strategy to alter polymer morphology, reduce aggregates in solution, and increase

polymer free volume for enhanced polymer–solvent interactions.

2. RESULTS AND DISCUSSION

As the effect of flexible linker on polymer solubility in nonhalogenated solvents has yet been studied, a linear linker (C_5) was synthesized as a control along with the two new branched linkers—one with an additional methyl group (C_5 M) and another with two ethyl groups (C_5 DE) (Figure 1). For a systematic study, all alkyl linkers were kept at five carbon atoms in length. Density functional theory (DFT) was used to calculate the optimized conformation and dihedral angle of the linker backbone. As shown in Figure 1, the C_5 linker has a dihedral angle of 180.0°, indicating a perfectly planar structure. C_5 M, on the other hand, is slightly bent from the methyl group to give a dihedral angle of 176.2°. The additional methyl group further introduces atacticity and regio-irregularity to the polymer backbone due to a lack of planar symmetry. Finally, C_5 DE is completely twisted with a dihedral angle of 108.3° and contains two chiral centers to give three stereoisomers—S–S, S–R, and R–R—which should greatly interrupt polymer packing and increase the polymer's free volume.

2.1. A Model Study: Fully Nonconjugated DPP Polymers. To assess the effect of linker nonlinearity on polymer morphology, the flexible linkers were polymerized with 3,6-bis(5-bromothiophene-2-yl)-N,N'-bis(5-decy-1-pentadecyl)-1,4-dioxopyrrolo[3,4-c]pyrrole (DPP monomer) in 1:1 molar ratio via Stille coupling to give nonconjugated polymers: DPP- C_5 , DPP- C_5 M, and DPP- C_5 DE. The polymers were purified by Soxhlet extraction using methanol, acetone, and hexanes to remove low molecular weight oligomers and impurities before extraction by chloroform to yield a dark blue

powder. Notably, DPP-C₅DE was a dark blue paste (Figure S7) and exhibited superior processability as it completely dissolved during hexanes Soxhlet extraction. The polymers showed comparable number-average molecular weight (M_n) of around 15 kg mol⁻¹, weight dispersity (D_w), and degree of polymerization (DP_n) as determined by high-temperature size-exclusion chromatography (SEC) at 180 °C (Table 1).

Grazing-incidence X-ray diffraction (GIXD) and differential scanning calorimetry (DSC) were performed on the polymers to probe molecular packing and physical properties such as crystallinity, glass transition temperature (T_g), and melting temperature (T_m). DPP-C₅ showed intense out-of-plane ($h00$) alkyl diffraction up to the fifth-order reflection and a strong (010) peak on the q_{xy} axis, indicating strong edge-on orientation and a high degree of crystallinity (Figure 2a).

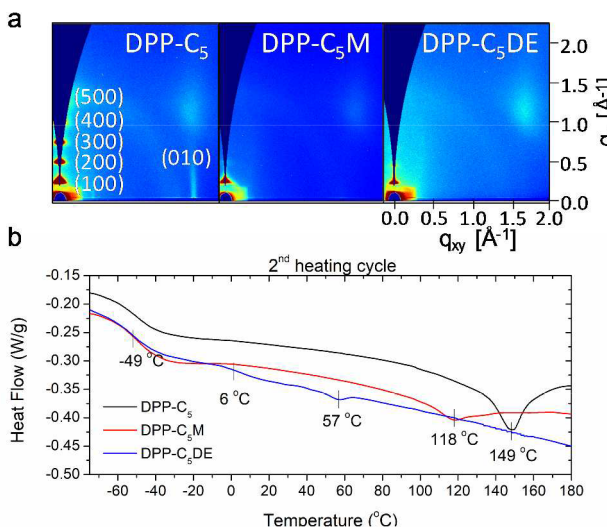


Figure 2. Physical properties of different fully nonconjugated DPP polymers. (a) 2D grazing-incidence X-ray diffraction (GIXD) patterns of the polymers spin-coated from 5 mg mL⁻¹ chlorobenzene solutions on Si substrates after annealing at 150 °C under nitrogen. All images were scaled for exposure time and illuminated volume for qualitative comparison across samples. (b) Differential scanning calorimetry (DSC) heating traces of the polymers.

DPP-C₅M and DPP-C₅DE, on the other hand, both showed weak (200) intensity and no obvious (010) π – π stacking peak, indicating low ordering and crystallinity. This is consistent with DSC data, which showed a decrease in the enthalpy of fusion (ΔH_{fus}) and T_m with increased branching (Table 1). This is likely due to the torsion introduced to the polymer backbone through the branched flexible linkers shown in DFT calculations, which greatly hinders π – π interactions between the DPP and thiophene units. DPP-C₅M and DPP-C₅DE are also atactic which exhibit low crystallinity relative to isotactic DPP-C₅. Aside from the side-chain T_g (~49 °C), a backbone T_g was also observed for DPP-C₅DE at 6 °C. Its T_m and ΔH_{fus} of 57 °C and 0.7 J g⁻¹, respectively, are both among the lowest reported for flexible linker polymers and may be good candidates for low-temperature melt processing method previously reported by Zhao et al.⁴⁶

The viscoelastic properties of the polymers at room temperature were examined using frequency sweep experiments. DPP-C₅ and DPP-C₅M both exhibited a plateau of storage (G') and loss (G'') moduli characteristic for linear elastic solids (Figure 3). DPP-C₅DE, on the contrary,

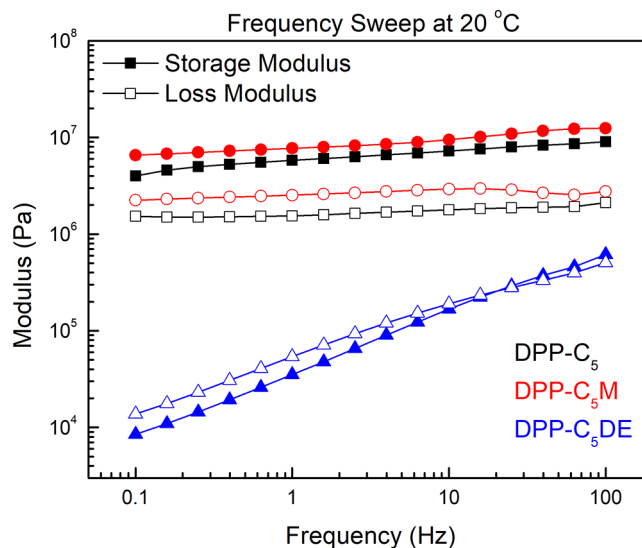


Figure 3. Frequency sweep at 0.5% strain and 20 °C of polymers with various flexible linkers. The loss modulus dominates at most frequencies for DPP-C₅DE, indicating liquid-like characteristics.

displayed heavily viscoelastic behavior at room temperature with G'' dominating at most frequencies and significantly lower moduli overall due to its subambient backbone T_g as well as the isomeric nature of the C₅DE linker, which further limits interchain interactions. This accounts for the soft paste-like appearance of the polymer.

2.2. Conjugated DPP Polymers with Branched Flexible Linkers. Encouraged by the drastic change in polymer physical properties when introducing atacticity and chirality through tertiary carbon atoms, DPP polymers with 10 mol % of flexible linker and 90 mol % 1,2-(E)-bis(5'-trimethylstannanyl-2'-C-thienyl)ethene (TVT monomer) were synthesized to give DPP-10C₅, DPP-10C₅M, and DPP-10C₅DE. Incorporation of 10 mol % flexible linker was selected, as previous studies showed negligible change in bandgap, HOMO–LUMO levels, and charge transport properties at this ratio.^{39,44} Fully conjugated DPPTVT was synthesized through the polymerization of a 1:1 equivalence of DPP/TVT monomer as a reference material to investigate the effect of introducing alkyl linkers on polymer processability. High-temperature SEC gave high M_n (~45 kg mol⁻¹) for all polymers with comparable number-average degree of polymerization $DP_n \sim 36$ (Table 2). Maintaining high and similar M_n is essential in this study as low- M_n polymers have lower solvation energy, making it difficult to evaluate the effectiveness of branched flexible linkers on polymer processability. The correct chemical composition and mol % of flexible linkers in the polymers were confirmed by ¹H NMR (Figure S4).

2.2.1. Physical Properties. GIXD images of the polymers showed strong edge-on orientation with ($h00$) lamella diffraction peaks up to the third-order and a weak (010) π – π stacking peak (Figure 4a). Unlike the fully nonconjugated polymers, the relative degree of crystallinity between the polymer films was not obvious initially. However, from the meridian linecut plots (Figure 4b), a sharp decrease in lamellar peak intensity was observed for DPP-10C₅M and DPP-10C₅DE relative to DPPTVT and DPP-10C₅. This is consistent with earlier X-ray results that showed a high degree of ordering for fully nonconjugated DPP-C₅, indicating that the linear alkyl linker C₅ is insufficient to disrupt polymer

Table 2. Molecular Weight and Physical Properties of the Different DPP Polymers with 10% Flexible Linker

polymer	x:y ^a	M_n (kg mol ⁻¹) ^b	M_w (kg mol ⁻¹) ^c	D_w ^d	DP_n ^e	T_g^1 (°C) ^f			T_g^2 (°C) ^g		
						DSC	$\tan \delta^h$	E''^i	DSC	$\tan \delta$	E''^j
DPPTVT	100:0	42.2	113.9	2.70	33.9	-43.2					
DPP-10C ₅	90:10	47.2	152.9	3.24	37.8	-44.0	-28.9	-40.6			81.1
DPP-10C ₅ M	90:10	46.0	116.8	2.54	36.8	-45.6	-28.1	-40.8	65.6		32.7
DPP-10C ₅ DE	90:10	44.1	101.9	2.31	34.1	-47.3	-30.2	-44.0	42.0	50.0	35.4

^aTVT: flexible linker monomer ratio. ^bNumber-average molecular weight. ^cWeight-average molecular weight. ^dWeight dispersity, defined as M_w/M_n . ^eDegree of polymerization. ^fSide-chain glass transition temperature. ^gBackbone glass transition temperature. ^hGlass transition temperature defined by $\tan \delta$ as measured by dynamic mechanical analysis. ⁱGlass transition temperature defined by the loss modulus (E'') as measured by dynamic mechanical analysis.

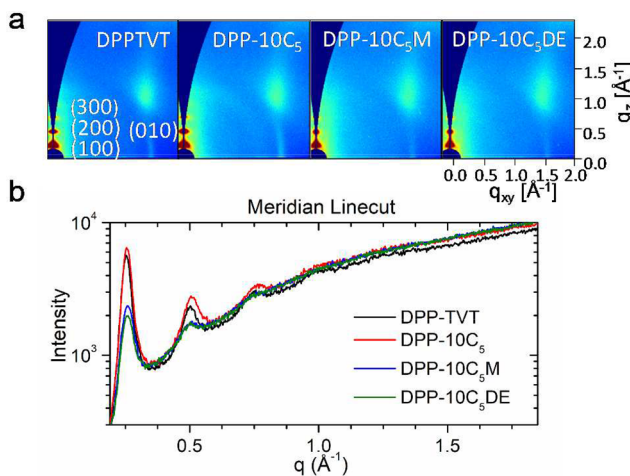


Figure 4. Grazing-incidence X-ray diffraction of different DPP polymers with 10% flexible linker. (a) GIXD diffractograms and (b) polarization-corrected meridian ($q_{xy} \approx 0$) line cuts of the polymers spin-coated from 5 mg mL⁻¹ chlorobenzene solutions on Si substrates with annealing at 150 °C under nitrogen. All images were scaled for exposure time and illuminated volume for qualitative comparison across samples. Detailed crystallographic parameters could be found in Table S1 of the Supporting Information.

crystallinity. C₅M and C₅DE linkers, on the other hand, due to their twisted structure, could suppress polymer crystallization by introducing kinks to the polymer backbone. Polymer crystallinity has implications on polymer solubility as the solvation enthalpy change must provide for the enthalpy change of fusion to melt crystallites.³⁷ Hence, a lower degree of crystallinity should aid in the dissolution of semicrystalline conjugated polymers.

UV-vis absorption spectra of the polymers in solution and thin film were measured (Figure 5) to investigate their aggregation and optoelectronic properties. A $\pi-\pi^*$ transition was recorded around 450 nm for all polymers in both states. Their internal charge transfer peak between 600 and 900 nm showed two distinct vibronic bands: the 0–1 and 0–0 transitions, with the lower energy 0–0 peak typically attributed to polymer aggregation.^{49,50} When normalized to the 0–1 vibronic peak, a gradual decrease in polymer aggregation was observed in solution with increased branching, suggesting better solvation of polymer chains. Interestingly, for the thin-film spectra, such a trend was not observed. A slight decrease in the 0–0 peak was only recorded for DPP-10C₅ and DPP-10C₅M, suggesting that a reduction of aggregation in solution does not necessarily translate in film state. This is promising, as strong short-range order was only disrupted in solution for enhanced processability but mostly maintained in film state for

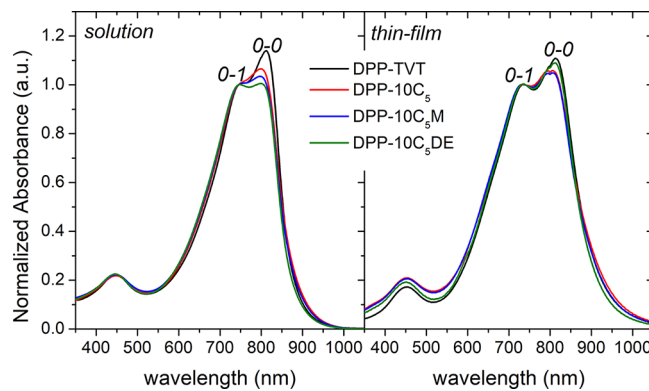


Figure 5. Normalized UV-vis absorption spectra of the various DPP polymers in 10⁻⁷ M chloroform solution (left) and spin-coated thin film on glass (right).

good charge transport.²² Not surprisingly, a small blue-shift was observed for all polymers relative to DPPTVT due to a decrease in conjugation length caused by the flexible linkers (Figure S28).

To better understand the effect of branching in flexible linkers on polymer chain dynamics and free volume, the T_g of the polymers were measured using DSC and dynamic mechanical analysis (DMA). The DSC and DMA measurements of DPP-10C₅DE are shown in Figure 6, and the results are summarized in Table 2. Detailed DSC and DMA curves for other polymers can be found in the Supporting Information (Figures S10–S15). As expected, no T_m was observed by DSC for all polymers, which is typical for most donor–acceptor (D–A) conjugated polymers due to their low crystallinity. A side-chain $T_g \sim -46$ °C was observed for all samples, but only DPP-10C₅DE exhibited a backbone T_g at 42 °C. The backbone T_g of the remaining polymers could only be measured by DMA temperature sweep experiments following reported procedures.³⁹ The T_g could be extracted either from a peak in $\tan \delta$ or from the loss modulus (E''); both values are included in Table 2. According to the values obtained for side-chain T_g , E'' corresponds closer to the values obtained from DSC compared to $\tan \delta$. A low backbone T_g of 81 °C was observed for DPP-10C₅ based on E'' , which is consistent with the literature³⁹ and attributed to an increase in backbone segmental motion from the nonconjugated flexible linker. DPP-10C₅M and DPP-C₅DE gave even lower backbone T_g of 33 and 35 °C, respectively, suggesting that even a small fraction of incorporated tertiary carbon atoms in the backbone is sufficient to increase the free volume of the conjugated polymers.

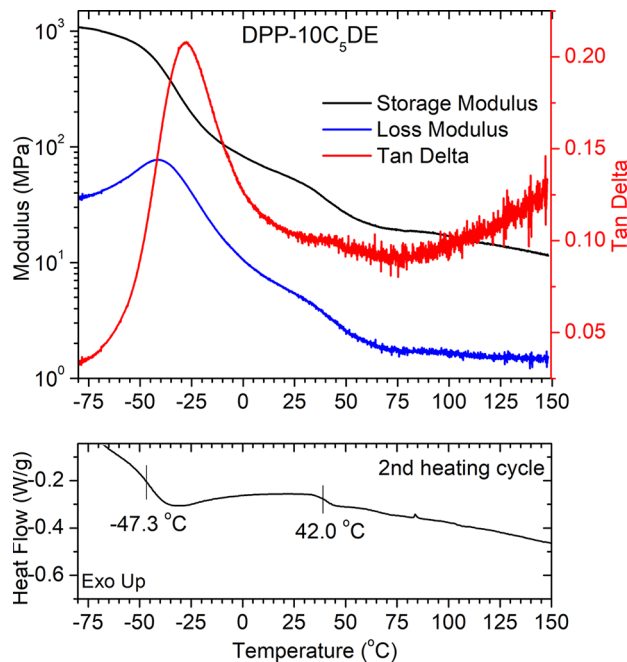


Figure 6. Dynamic mechanical analysis (DMA) temperature sweep showing the storage modulus (E'), loss modulus (E''), and $\tan \delta$ (top) and DSC heating trace (bottom) of DPP-10C₅DE.

2.2.2. Polymer Processability. As an initial evaluation of processability, the polymers were dissolved in hot 1,2-dichlorobenzene (*o*-DCB), a common chlorinated processing solvent for conjugated polymers, at 20 mg mL⁻¹. DPPTVT

could not be dissolved at such a high concentration; hence, a lower M_n (28 kg mol⁻¹) batch was prepared with a 1:0.9 equivalence of DPP/TVT monomer to give DPPTVT-28k, which was dissolved at 10 mg mL⁻¹. Upon cooling to room temperature DPPTVT-28k and DPP-10C₅ formed gels after 10 min, whereas DPP-10C₅M partially gelled, and DPP-10C₅DE maintained a homogeneous solution (Figure 7a). For a more quantitative evaluation of the polymer inks, their viscosities were measured by rotational rheometry at various shear rates (Figure 7b). Aside from DPP-10C₅—which showed a high viscosity of 1.4 Pa s at a shear strain rate of 10 s⁻¹ and a gradual decrease to 0.15 Pa s at 100 s⁻¹ due to shear thinning—all polymers behaved as Newtonian fluids with negligible change in viscosity in the shear sweep experiment. DPP-10C₅DE gave the lowest viscosity at 9 × 10⁻³ Pa s across all measured shear rates, likely due to low aggregation and a larger free volume.

To evaluate the branched linker's effect on solvation, the polymers were dissolved in *p*-xylene, a nonpolar industrial solvent. The solubility limit of each polymer in *p*-xylene was calculated via UV-vis spectroscopy following a previous report.^{25,35} Known concentrations of 0.001–0.010 mg mL⁻¹ in *p*-xylene were measured first to generate a linear plot of polymer concentration to the absorption maxima by the Beer-Lambert law (Figure 7c). A saturated polymer solution in *p*-xylene at 80 °C was then diluted 3000-fold, and its UV-vis absorption was measured. Based on the maximum absorption and linear plot, the polymer saturated concentration could then be extrapolated. As shown in Table 3, the solubility limit of DPPTVT in *p*-xylene was merely 1.0 mg mL⁻¹. DPPTVT-

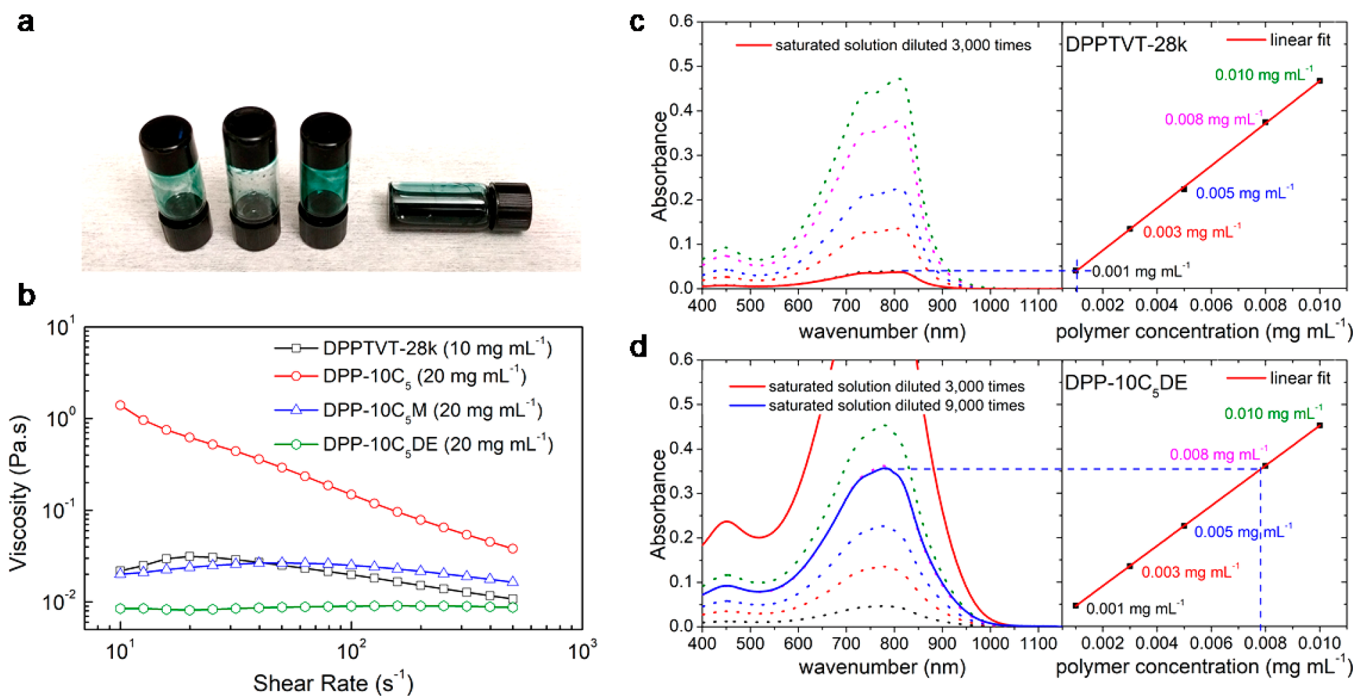


Figure 7. Solution processability of different DPP polymers with 10% flexible linker. (a) Photograph of DPPTVT-28k, DPP-10C₅, DPP-10C₅M, and DPP-10C₅DE (left to right) in 20 mg mL⁻¹ *o*-DCB and (b) their respective shear sweep viscosity measurements. DPPTVT-28k was dissolved in 10 mg mL⁻¹ *o*-DCB. UV-vis concentration analysis of (c) DPPTVT-28k and (d) DPP-10C₅DE in *p*-xylene. The left panels show the absorption spectra of DPPTVT-28k and DPP-10C₅DE at concentrations 1.0, 3.0, 5.0, and 10.0 $\mu\text{g mL}^{-1}$ and saturated solutions prepared at 80 °C diluted 3000-fold or 9000-fold (solid lines). The right panels show a linear fit of the polymer concentrations plotted against their absorption maxima. By the Beer-Lambert law, the concentrations of the diluted saturated polymer solutions were calculated. The UV-vis concentration analysis of other polymers could be found in the Supporting Information (Figures S16–S19).

Table 3. Calculated Solubility Limits of DPP Polymers in *p*-Xylene via UV–Vis Analysis

polymer	saturated concn in <i>p</i> -xylene (mg mL ⁻¹)
DPPTVT	1.0
DPPTVT-28k	3.0
DPP-10C ₅	8.1
DPP-10C ₅ M	23.8
DPP-10C ₅ DE	70.9; 20.6 (in 2-mTHF) ^a

^aSaturated concentration of DPP-10C₅DE in 2-methyltetrahydrofuran.

28k showed a marginal improvement of 3.0 mg mL⁻¹ due to a decrease in M_n . However, by incorporating 10% of flexible linker, the solubility limits were elevated to 8.1 and 23.8 mg mL⁻¹ for DPP-10C₅ and DPP-10C₅M, respectively. DPP-10C₅DE gave the highest solubility limit of 70.9 mg mL⁻¹, which is 70 times higher than the reference polymer DPPTVT. The saturated polymer solution had to be diluted 9000-fold to obtain an absorption maximum within the linear plot range (Figure 7d). Its solubility limit in 2-methyltetrahydrofuran (2-mTHF), a popular polar green substitute for tetrahydrofuran, was also measured and calculated to be 20.6 mg mL⁻¹. The superior solubility of DPP-10C₅DE could be attributed to its isomeric flexible linker, which reduces intermolecular interactions and the polymer's propensity to form aggregates in solution.⁵¹ Furthermore, its longer branching gives the polymer a larger free volume for solvent interactions.

2.2.3. Charge Transport Properties. Aside from solvation, the effect of branched flexible linkers on polymer charge transport is also critical. The field-effect hole mobility (μ_h) of the polymers was measured by preparing OFET devices with a bottom-gate/top-contact (BGTC) configuration on *n*-octadecyltrimethoxysilane (OTMS)-modified SiO₂/Si substrates. Solution shearing and inkjet printing were selected as the deposition methods due to their compatibility with roll-to-

roll processes and their ability to enhance charge transport through preferential polymer alignment in a specific direction.^{8,52–57} Solution shearing allows for efficient large-area printing, and inkjet printing permits microscale patterning. Furthermore, while there are several reports of OFETs prepared through spin coating of industrial solvents, there is still little work on environmentally benign solvent printed OFETs.

The conditions that gave the best device performance for each solvent and deposition method are summarized in Table 4. For simplification and better comparison of film quality achieved by the different solvents, only the device characteristics and charge transport along the coating direction are shown in Table 4 for the solution-sheared films, which exhibited higher μ_h in the tested conditions. OFET device characteristics in the direction perpendicular to shearing and other shearing speed tested can be found in the Supporting Information (Tables S2–S7). While Table 4 shows the best conditions tested in this study for different solvents and deposition methods, the film quality is not yet optimal, as there are still many parameters (temperature, concentration, blade architecture, etc.) that could be tuned to improve polymer chain alignment, which falls out of the scope of this study.

The polymers were first solution-sheared using chlorobenzene (CB) as a point of comparison, which typically gives high performance and uniform films due to excellent polymer solubility.^{58–60} Based on cross-polarized optical microscopy, polarized UV–vis spectroscopy, and μ_h anisotropy, chain alignment in the direction of shearing was observed for all polymers except for DPP-10C₅ (Figure S20). Birefringent films were obtained according to cross-polarized images, and a dichroic ratio $R > 1.0$ was recorded indicating a preferential alignment in the direction of shearing (Table 4). The dichroic ratio R was defined as the absorption of the polymer 0–0 peak in the direction parallel to shearing divided by that in the perpendicular direction ($R = A_{\parallel}/A_{\perp}$). As shown in Table 4, a

Table 4. OFET Device Characteristics of DPP Polymers in BGTC Configuration Using Various Solvents and Deposition Conditions^a

polymer	solvent	deposition process	substrate	temp (°C)	concn (mg mL ⁻¹)	deposition condition ^b	μ_h (cm ² V ⁻¹ s ⁻¹) ^c		V_{th}^e (V) ^e	R^f
							avg	max		
DPPTVT-28k	CB	solution shearing	OTMS ^g	50	15	0.50 mm s ⁻¹	1.88	2.22	>10 ⁶	-5.5
DPP-10C ₅	CB	solution shearing	OTMS	50	15	0.50 mm s ⁻¹	1.12	1.17	>10 ⁶	-2.5
DPP-10C ₅ M	CB	solution shearing	OTMS	50	15	0.50 mm s ⁻¹	1.52	1.94	>10 ⁵	2.3
DPP-10C ₅ DE	CB	solution shearing	OTMS	50	20	0.25 mm s ⁻¹	1.68	2.04	>10 ⁴	5.1
	tetralin	solution shearing	OTMS	50	22	0.025 mm s ⁻¹	2.17	2.76	>10 ⁵	-4.9
	mesitylene	solution shearing	OTMS	40	22	0.08 mm s ⁻¹	1.71	2.03	>10 ⁵	0.7
	<i>p</i> -xylene	solution shearing	OTMS	40	22	0.10 mm s ⁻¹	1.17	1.69	>10 ⁵	-3.7
	2-mTHF	solution shearing	OTMS	55	10	1.00 mm s ⁻¹	0.81	1.02	>10 ⁶	12.4
	<i>o</i> -MA	solution shearing	BCB ^h	80	10	0.25 mm s ⁻¹	0.17	0.22	>10 ⁵	0.0
	<i>o</i> -MA	spin coating	BCB	25	10	2200 rpm	0.04	0.05	>10 ⁴	-4.0
	tetralin	spin coating	BCB	25	5	1200 rpm	0.36	0.41	>10 ⁵	-2.8
	tetralin	inkjet printing	BCB	55	13	35 μm dtd	0.46	0.52	>10 ³	-1.2

^aAll polymer thin films were thermally annealed at 150 °C for 30 min under nitrogen before measurement. All values are averaged and extracted from at least six devices. For solution-sheared devices, the parallel-to-shearing-direction transport characteristics are given. ^bDeposition condition of the best device characteristics achieved for each solvent and deposition method. The shear rate, spin rate, and drop-to-drop distance are shown for solution shearing, spin coating, and inkjet printing, respectively. Device characteristics of all deposition conditions attempted in this study are in the Supporting Information (Tables S2–S8). ^cField-effect hole mobility. ^dOn–off ratio of the device. ^eThreshold voltage of the device. ^fDichroic ratio (R) defined by maximum polarized UV–vis absorption in parallel to shearing direction divided by that in perpendicular to shearing direction. ^g*n*-Octadecyltrimethoxysilane monolayer on 300 nm SiO₂ substrates. ^hBenzocyclobutene layer on 300 nm SiO₂ substrates.

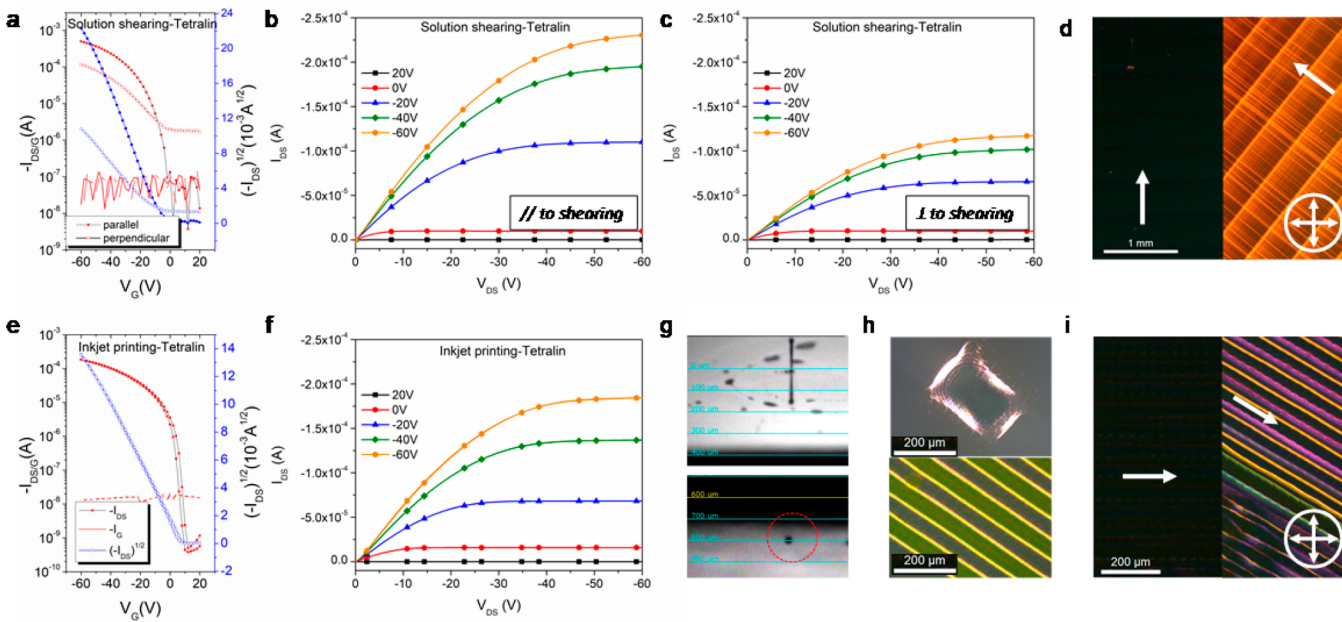


Figure 8. OFET characteristics and alignment of solution-sheared and inkjet-printed **DPP-10C₅DE** device in the BGTC configuration ($L = 50 \mu\text{m}$, $W = 1000 \mu\text{m}$). The source-drain voltage was set to be -60 V for all measurements. (a) Transfer and (b, c) output curves of tetralin sheared films for both the parallel (II) and perpendicular (I) to shearing orientations. Cross-polarized optical microscope images of (d) solution-sheared and (i) inkjet-printed polymer films. Blue arrows indicate printing direction, and crossed arrows indicate orientation of cross-polarizers. (e) Transfer and (f) output curves of inkjet-printed films. (g) Inkjet-printed drop profile at $20 \mu\text{s}$ (top) and $125 \mu\text{s}$ (bottom). (h) Inkjet-printed rectangle (top) and lines (bottom).

maximum μ_h of $2.22 \text{ cm}^2 \text{ V}^{-1} \text{ s}^{-1}$ was achieved for **DPPTVT-28k**. DPPTVT solution could not be sheared to give a uniform film with sufficient thickness (at least 20 nm) due to its poor solubility. As anticipated, the polymers with 10 mol % flexible linkers still exhibited excellent semiconducting properties. **DPP-10C₅M** and **DPP-10C₅DE** gave similar μ_h at 1.94 and $2.04 \text{ cm}^2 \text{ V}^{-1} \text{ s}^{-1}$, respectively, despite a decrease in crystallinity. The high μ_h was likely maintained due to the high M_n and aggregation shown by UV-vis in the polymer films.^{22,23} A slight decrease in μ_h was recorded for **DPP-10C₅** at $1.17 \text{ cm}^2 \text{ V}^{-1} \text{ s}^{-1}$, likely due to a lack of alignment and deposition-induced ordering. No birefringence was observed, and a dichroic ratio of $R = 1.0$ was measured (Table S2 and Figure S20).

The exceptional processability of **DPP-10C₅DE** was illustrated by solution shearing with several nonhalogenated solvents. Tetralin, mesitylene, and *p*-xylene polymer inks displayed outstanding polymer–solvent interaction and were sheared at a high concentration of 22 mg mL^{-1} with high μ_h ($\sim 2.0 \text{ cm}^2 \text{ V}^{-1} \text{ s}^{-1}$) comparable to what was achieved using CB. A typical transfer and output curve of solution-sheared **DPP-10C₅DE** in orientations both parallel and perpendicular to shearing and its cross-polarized image are presented in Figure 8. Tetralin gave the highest μ_h of $2.76 \text{ cm}^2 \text{ V}^{-1} \text{ s}^{-1}$, showing good alignment along the shearing direction based on polarized optical microscopy, polarized UV-vis (dichroic ratio $R = 1.3$), and a high μ_h anisotropy of 4.9 (Figure 8a–d). *p*-Xylene, a more industry-friendly solvent with a low NFPA rating of 1 for health hazard, gave a maximum μ_h of $1.69 \text{ cm}^2 \text{ V}^{-1} \text{ s}^{-1}$ with a dichroic ratio of 1.3 . 2-mTHF and 2-methylanisole (*o*-MA) were also examined and gave respectable μ_h of 1.02 and $0.22 \text{ cm}^2 \text{ V}^{-1} \text{ s}^{-1}$, respectively. *o*-MA is a benign food additive with an NFPA rating of 0 for health hazard and was previously used to coat polymer semiconductor

blends for OPVs.¹⁸ However, due to their poor wettability, both *o*-MA and 2-mTHF showed limited layer coverage and no alignment in the tested conditions. The *o*-MA polymer solution could only be sheared on benzocyclobutene (BCB)-modified substrates, which has a lower contact angle but typically gave lower μ_h compared to OTMS substrates. Possibly due to its limited solubility, films prepared by shearing as well as spin-coating in *o*-MA showed low uniformity and higher film roughness (Figure S25), which accounts for the compromised device characteristics.

DPP-10C₅DE was further applied to inkjet printing to test its applicability in patterning techniques. Tetralin was selected as the solvent for its high boiling point ($\sim 207^\circ\text{C}$), which allows elevated processing temperatures without the worry of clogging the $21.5 \mu\text{m}$ wide nozzle from solvent evaporation. The polymer ink was prepared at a concentration of 13 mg mL^{-1} and filtered through a $0.45 \mu\text{m}$ Teflon filter prior to printing. As shown in Figure 8g,h, the ink showed stable jetting during printing process and excellent printability to give rectangles and lines. Furthermore, due to the high concentration, only a single printed layer was required to give a continuous and uniform film on BCB substrates with a μ_h of $0.52 \text{ cm}^2 \text{ V}^{-1} \text{ s}^{-1}$. A representative transfer and output curve is shown in Figure 8e,f. Surprisingly, the μ_h measured was greater than what was obtained for a film prepared from spin coating on BCB (Table 4), possibly due to the alignment that came from the directional drying along the printing direction (Figure 8i). This is promising as the high processability of the polymer has enabled inkjet printing to pattern and boost charge carrier mobility simultaneously through polymer alignment, which is highly attractive for low-cost fabrication of plastic electronics.

3. CONCLUSION

In summary, we synthesized two branched nonconjugated flexible linkers, C_5M and C_5DE , incorporated them into conjugated DPP polymers, and revealed an effective and versatile approach to enhance polymer processability in benign solvents. DFT calculations revealed that the insertion of tertiary carbon atoms to alkyl linkers could lead to significant bending and torsion to conjugated backbones. This was consistent with GIXD studies and solution UV-vis which showed a decrease in polymer crystallinity and aggregation relative to fully conjugated DPPTVT and DPP-10C₅. DSC and DMA experiments revealed a suppression in backbone T_g indicating an increase in the free volume of the polymers with branched alkyl linkers. Rheology measurements revealed that polymer solution viscosity was directly proportional to the amount of branching in the flexible linkers. Owing to the synergistic effect of decreased crystallinity and solution aggregates and increased free volume, the solubility limits for DPP-10C₅M and DPP-10C₅DE in the benign solvent *p*-xylene are respectively 23- and 70-fold greater than that of the reference polymer DPPTVT. DPP-10C₅DE thin films were successfully deposited by solution shearing at high concentrations for both polar and nonpolar benign solvents for OFETs to give a maximum μ_h of $2.76\text{ cm}^2\text{ V}^{-1}\text{ s}^{-1}$. Polymer inks in tetralin showed high stability and were inkjet-printed to give μ_h of $0.52\text{ cm}^2\text{ V}^{-1}\text{ s}^{-1}$. Branched alkyl linkers are found to be a powerful tool to strengthen solvent interactions of high-performance polymer semiconductors with minimal compromise in charge carrier mobility, which activates their true potential in low-cost, lightweight, and eco-friendly printed electronics.

■ ASSOCIATED CONTENT

Supporting Information

The Supporting Information is available free of charge on the ACS Publications website at DOI: [10.1021/acs.macromol.8b00971](https://doi.org/10.1021/acs.macromol.8b00971).

Synthesis, NMR, high-temperature SEC, DFT calculations, GIXD data, DSC, DMA, UV-vis concentration analysis, additional transistor characteristics, cross-polarized optical images, and ink viscosity measurements ([PDF](#))

■ AUTHOR INFORMATION

Corresponding Author

*E-mail: zbao@stanford.edu (Z.B.).

ORCID

Ging-Ji Nathan Wang: [0000-0002-5432-3046](https://orcid.org/0000-0002-5432-3046)

Hung-Chin Wu: [0000-0001-6492-0525](https://orcid.org/0000-0001-6492-0525)

Leo Shaw: [0000-0003-1182-5537](https://orcid.org/0000-0003-1182-5537)

Zhenan Bao: [0000-0002-0972-1715](https://orcid.org/0000-0002-0972-1715)

Notes

The authors declare no competing financial interest.

■ ACKNOWLEDGMENTS

This work was supported by the Air Force Office of Scientific Research (FA9550-15-1-0106 & FA9550-18-1-0143). The authors thank Prof. Bob C. Schroeder for assistance in ESI-MS measurements. F.M.-L. was partly supported by the Swiss National Science Foundation under the Early Mobility Postdoc Project P2ELP2_155355. H.C.W. acknowledges the financial

support for postdoctoral oversea research program from the Ministry of Science and Technology of Taiwan (MOST 106-2917-I-564-023). J.L. acknowledges support by the National Science Foundation Graduate Research Fellowship Program under Grant DGE-114747. L.S. acknowledges support from the Kodak Graduate Fellowship. Part of this work was performed at the Stanford Nano Shared Facilities (SNSF), supported by the National Science Foundation under Award ECCS-1542152. Use of the Stanford Synchrotron Radiation Lightsource, SLAC National Accelerator Laboratory, is supported by the U.S. Department of Energy, Office of Science, Office of Basic Energy Sciences under Contract No. DE-AC02-76SF00515.

■ REFERENCES

- (1) Lipomi, D. J.; Bao, Z. Stretchable and Ultraflexible Organic Electronics. *MRS Bull.* **2017**, *42* (02), 93–97.
- (2) Wang, G.-J. N.; Gasperini, A.; Bao, Z. Stretchable Polymer Semiconductors for Plastic Electronics. *Adv. Electron. Mater.* **2018**, *4*, 1700429.
- (3) Lee, Y.; Shin, M.; Thiagarajan, K.; Jeong, U. Approaches to Stretchable Polymer Active Channels for Deformable Transistors. *Macromolecules* **2016**, *49* (2), 433–444.
- (4) Chortos, A.; Liu, J.; Bao, Z. Pursuing Prosthetic Electronic Skin. *Nat. Mater.* **2016**, *15* (9), 937–950.
- (5) Someya, T.; Bao, Z.; Malliaras, G. G. The Rise of Plastic Bioelectronics. *Nature* **2016**, *540* (7633), 379–385.
- (6) Irimia-Vladu, M.; Troshin, P. A.; Reisinger, M.; Shmygleva, L.; Kanbur, Y.; Schwabegger, G.; Bodea, M.; Schwödauer, R.; Mumyatov, A.; Fergus, J. W.; et al. Biocompatible and Biodegradable Materials for Organic Field-Effect Transistors. *Adv. Funct. Mater.* **2010**, *20* (23), 4069–4076.
- (7) Lei, T.; Guan, M.; Liu, J.; Lin, H.-C.; Pfattner, R.; Shaw, L.; McGuire, A. F.; Huang, T.-C.; Shao, L.; Cheng, K.-T.; et al. Biocompatible and Totally Disintegrable Semiconducting Polymer for Ultrathin and Ultralightweight Transient Electronics. *Proc. Natl. Acad. Sci. U. S. A.* **2017**, *114* (20), 5107–5112.
- (8) Diao, Y.; Shaw, L.; Bao, Z.; Mannsfeld, S. C. B. Morphology Control Strategies for Solution-Processed Organic Semiconductor Thin Films. *Energy Environ. Sci.* **2014**, *7* (7), 2145–2159.
- (9) Søndergaard, R. R.; Hösel, M.; Krebs, F. C. Roll-to-Roll Fabrication of Large Area Functional Organic Materials. *J. Polym. Sci., Part B: Polym. Phys.* **2013**, *51* (1), 16–34.
- (10) Sirringhaus, H.; Kawase, T.; Friend, R. H.; Shimoda, T.; Inbasekaran, M.; Wu, W.; Woo, E. P. High-Resolution Inkjet Printing of All-Polymer Transistor Circuits. *Science (Washington, DC, U. S.)* **2000**, *290* (5499), 2123–2126.
- (11) Forrest, S. R. The Path to Ubiquitous and Low-Cost Organic Electronic Appliances on Plastic. *Nature* **2004**, *428* (6986), 911–918.
- (12) Li, J.; Zhao, Y.; Tan, H. S.; Guo, Y.; Di, C.-A.; Yu, G.; Liu, Y.; Lin, M.; Lim, S. H.; Zhou, Y.; Su, H.; Ong, B. S. A Stable Solution-Processed Polymer Semiconductor with Record High-Mobility for Printed Transistors. *Sci. Rep.* **2012**, *2* (1), 754.
- (13) Kang, L.; Yun, H.-J.; Chung, D. S.; Kwon, S.-K.; Kim, Y.-H. Record High Hole Mobility in Polymer Semiconductors via Side-Chain Engineering. *J. Am. Chem. Soc.* **2013**, *135* (40), 14896–14899.
- (14) Liu, Y.; Zhao, J.; Li, Z.; Mu, C.; Ma, W.; Hu, H.; Jiang, K.; Lin, H.; Ade, H.; Yan, H. Aggregation and Morphology Control Enables Multiple Cases of High-Efficiency Polymer Solar Cells. *Nat. Commun.* **2014**, *5* (1), 5293.
- (15) Gu, X.; Shaw, L.; Gu, K.; Toney, M. F.; Bao, Z. The Meniscus-Guided Deposition of Semiconducting Polymers. *Nat. Commun.* **2018**, *9* (1), 534.
- (16) Zhou, Y.; Gu, K. L.; Gu, X.; Kurosawa, T.; Yan, H.; Guo, Y.; Koleilat, G. I.; Zhao, D.; Toney, M. F.; Bao, Z. All-Polymer Solar Cells Employing Non-Halogenated Solvent and Additive. *Chem. Mater.* **2016**, *28* (14), 5037–5042.

- (17) Zhang, S.; Ye, L.; Zhang, H.; Hou, J. Green-Solvent-Processable Organic Solar Cells. *Mater. Mater. Today* **2016**, *19* (9), 533–543.
- (18) Zhang, H.; Yao, H.; Zhao, W.; Ye, L.; Hou, J. High-Efficiency Polymer Solar Cells Enabled by Environment-Friendly Single-Solvent Processing. *Adv. Energy Mater.* **2016**, *6* (6), 1502177.
- (19) Xu, X.; Yu, T.; Bi, Z.; Ma, W.; Li, Y.; Peng, Q. Realizing Over 13% Efficiency in Green-Solvent-Processed Nonfullerene Organic Solar Cells Enabled by 1,3,4-Thiadiazole-Based Wide-Bandgap Copolymers. *Adv. Mater.* **2018**, *30* (3), 1703973.
- (20) Ye, L.; Xiong, Y.; Yao, H.; Gadisa, A.; Zhang, H.; Li, S.; Ghasemi, M.; Balar, N.; Hunt, A.; O'Connor, B. T.; et al. High Performance Organic Solar Cells Processed by Blade Coating in Air from a Benign Food Additive Solution. *Chem. Mater.* **2016**, *28* (20), 7451–7458.
- (21) Zhao, W.; Zhang, S.; Zhang, Y.; Li, S.; Liu, X.; He, C.; Zheng, Z.; Hou, J. Environmentally Friendly Solvent-Processed Organic Solar Cells That Are Highly Efficient and Adaptable for the Blade-Coating Method. *Adv. Mater.* **2018**, *30* (4), 1704837.
- (22) Noriega, R.; Rivnay, J.; Vandewal, K.; Koch, F. P. V.; Stingelin, N.; Smith, P.; Toney, M. F.; Salleo, A. A General Relationship between Disorder, Aggregation and Charge Transport in Conjugated Polymers. *Nat. Mater.* **2013**, *12* (11), 1038–1044.
- (23) Zhang, X.; Bronstein, H.; Kronemeijer, A. J.; Smith, J.; Kim, Y.; Kline, R. J.; Richter, L. J.; Anthopoulos, T. D.; Sirringhaus, H.; Song, K.; et al. Molecular Origin of High Field-Effect Mobility in an Indacenodithiophene–benzothiadiazole Copolymer. *Nat. Commun.* **2013**, *4*, 1–9.
- (24) Cho, J.; Yu, S. H.; Chung, D. S. Environmentally Benign Fabrication Processes for High-Performance Polymeric Semiconductors. *J. Mater. Chem. C* **2017**, *5*, 2745–2757.
- (25) Venkateshvaran, D.; Nikolka, M.; Sadhanala, A.; Lemaur, V.; Zelazny, M.; Kepa, M.; Hurhangee, M.; Kronemeijer, A. J.; Pecunia, V.; Nasrallah, I.; et al. Approaching Disorder-Free Transport in High-Mobility Conjugated Polymers. *Nature* **2014**, *515* (7527), 384–388.
- (26) Patterson, D. Free Volume and Polymer Solubility. A Qualitative View. *Macromolecules* **1969**, *2* (6), 672–677.
- (27) Barton, A. F. M. Solubility Parameters. *Chem. Rev.* **1975**, *75* (6), 731–753.
- (28) Lei, T.; Wang, J. Y.; Pei, J. Roles of Flexible Chains in Organic Semiconducting Materials. *Chem. Mater.* **2014**, *26* (1), 594–603.
- (29) Mei, J.; Bao, Z. Side Chain Engineering in Solution-Processable Conjugated Polymers. *Chem. Mater.* **2014**, *26* (1), 604–615.
- (30) Fang, L.; Zhou, Y.; Yao, Y. X.; Diao, Y.; Lee, W. Y.; Appleton, A. L.; Allen, R.; Reinschamp, J.; Mannsfeld, S. C. B.; Bao, Z. Side-Chain Engineering of Isoindigo-Containing Conjugated Polymers Using Polystyrene for High-Performance Bulk Heterojunction Solar Cells. *Chem. Mater.* **2013**, *25* (24), 4874–4880.
- (31) Matthews, J. R.; Niu, W. J.; Tandia, A.; Wallace, A. L.; Hu, J. Y.; Lee, W. Y.; Giri, G.; Mannsfeld, S. C. B.; Xie, Y. T.; Cai, S. C.; et al. Scalable Synthesis of Fused Thiophene-Diketopyrrolopyrrole Semiconducting Polymers Processed from Nonchlorinated Solvents into High Performance Thin Film Transistors. *Chem. Mater.* **2013**, *25* (5), 782–789.
- (32) Shao, M.; He, Y.; Hong, K.; Rouleau, C. M.; Geohegan, D. B.; Xiao, K. A Water-Soluble Polythiophene for Organic Field-Effect Transistors. *Polym. Chem.* **2013**, *4* (20), 5270.
- (33) Lu, K.; Guo, Y.; Liu, Y.; Di, C.; Li, T.; Wei, Z.; Yu, G.; Du, C.; Ye, S. Novel Functionalized Conjugated Polythiophene with Oxetane Substituents: Synthesis, Optical, Electrochemical, and Field-Effect Properties. *Macromolecules* **2009**, *42* (9), 3222–3226.
- (34) Kanimozhi, C.; Yaacobi-Gross, N.; Chou, K. W.; Amassian, A.; Anthopoulos, T. D.; Patil, S. Diketopyrrolopyrrole–Diketopyrrolopyrrole-Based Conjugated Copolymer for High-Mobility Organic Field-Effect Transistors. *J. Am. Chem. Soc.* **2012**, *134* (40), 16532–16535.
- (35) Lee, S. M.; Lee, H. R.; Han, A.-R.; Lee, J.; Oh, J. H.; Yang, C. High-Performance Furan-Containing Conjugated Polymer for Environmentally Benign Solution Processing. *ACS Appl. Mater. Interfaces* **2017**, *9* (18), 15652–15661.
- (36) Yun, H.-J.; Lee, G. B.; Chung, D. S.; Kim, Y.-H.; Kwon, S.-K. Novel Diketopyrrolopyrrole Random Copolymers: High Charge-Carrier Mobility from Environmentally Benign Processing. *Adv. Mater.* **2014**, *26* (38), 6612–6616.
- (37) Choi, H. H.; Baek, J. Y.; Song, E.; Kang, B.; Cho, K.; Kwon, S.-K.; Kim, Y.-H. A Pseudo-Regular Alternating Conjugated Copolymer Using an Asymmetric Monomer: A High-Mobility Organic Transistor in Nonchlorinated Solvents. *Adv. Mater.* **2015**, *27* (24), 3626–3631.
- (38) Ji, Y.; Xiao, C.; Wang, Q.; Zhang, J.; Li, C.; Wu, Y.; Wei, Z.; Zhan, X.; Hu, W.; Wang, Z.; et al. Asymmetric Diketopyrrolopyrrole Conjugated Polymers for Field-Effect Transistors and Polymer Solar Cells Processed from a Nonchlorinated Solvent. *Adv. Mater.* **2016**, *28* (5), 943–950.
- (39) Schroeder, B. C.; Chiu, Y.-C.; Gu, X.; Zhou, Y.; Xu, J.; Lopez, J.; Lu, C.; Toney, M. F.; Bao, Z. Non-Conjugated Flexible Linkers in Semiconducting Polymers: A Pathway to Improved Processability without Compromising Device Performance. *Adv. Electron. Mater.* **2016**, *2* (7), 1600104.
- (40) Zhao, Y.; Zhao, X.; Zang, Y.; Di, C.; Diao, Y.; Mei, J. Conjugation-Break Spacers in Semiconducting Polymers: Impact on Polymer Processability and Charge Transport Properties. *Macromolecules* **2015**, *48* (7), 2048–2053.
- (41) Gasperini, A.; Bivaud, S.; Sivila, K. Controlling Conjugated Polymer Morphology and Charge Carrier Transport with a Flexible-Linker Approach. *Chem. Sci.* **2014**, *5* (12), 4922–4927.
- (42) Gasperini, A.; Jeanbourquin, X. A.; Rahamanudin, A.; Yu, X.; Sivila, K. Enhancing the Thermal Stability of Solution-Processed Small-Molecule Semiconductor Thin Films Using a Flexible Linker Approach. *Adv. Mater.* **2015**, *27* (37), 5541–5546.
- (43) Zhao, M.; Hashimoto, K.; Tajima, K. Synthesis of Copolymer Based on Naphthalene Diimide Connected with a Non-Conjugated Flexible Linker. *Synth. Met.* **2013**, *175*, 9–14.
- (44) Oh, J. Y.; Rondeau-Gagné, S.; Chiu, Y.; Chortos, A.; Lissel, F.; Wang, G.-J. N.; Schroeder, B. C.; Kurosawa, T.; Lopez, J.; Katsumata, T.; et al. Intrinsically Stretchable and Healable Semiconducting Polymer for Organic Transistors. *Nature* **2016**, *539* (7629), 411–415.
- (45) Zhao, Y.; Gumusengen, A.; He, J.; Qu, G.; McNutt, W. W.; Long, Y.; Zhang, H.; Huang, L.; Diao, Y.; Mei, J. Continuous Melt-Drawing of Highly Aligned Flexible and Stretchable Semiconducting Microfibers for Organic Electronics. *Adv. Funct. Mater.* **2018**, *28*, 1705584.
- (46) Zhao, Y.; Zhao, X.; Roders, M.; Gumusengen, A.; Ayzner, A. L.; Mei, J. Melt-Processing of Complementary Semiconducting Polymer Blends for High Performance Organic Transistors. *Adv. Mater.* **2017**, *29* (6), 1605056.
- (47) Zhao, X.; Zhao, Y.; Ge, Q.; Butrouna, K.; Diao, Y.; Graham, K. R.; Mei, J. Complementary Semiconducting Polymer Blends: The Influence of Conjugation-Break Spacer Length in Matrix Polymers. *Macromolecules* **2016**, *49* (7), 2601–2608.
- (48) Zhao, X.; Xue, G.; Qu, G.; Singhania, V.; Zhao, Y.; Butrouna, K.; Gumusengen, A.; Diao, Y.; Graham, K. R.; Li, H.; et al. Complementary Semiconducting Polymer Blends: Influence of Side Chains of Matrix Polymers. *Macromolecules* **2017**, *50* (16), 6202–6209.
- (49) Lei, Y.; Deng, P.; Li, J.; Lin, M.; Zhu, F.; Ng, T.; Lee, C.; Ong, B. S. Solution-Processed Donor-Acceptor Polymer Nanowire Network Semiconductors For High-Performance Field-Effect Transistors. *Sci. Rep.* **2016**, *6* (1), 24476.
- (50) Xu, J.; Wang, S.; Wang, G.-J. N.; Zhu, C.; Luo, S.; Jin, L.; Gu, X.; Chen, S.; Feig, V. R.; To, J. W. F.; et al. Highly Stretchable Polymer Semiconductor Films through the Nanoconfinement Effect. *Science (Washington, DC, U. S.)* **2017**, *355* (6320), 59–64.
- (51) Kim, B.-G.; Jeong, E. J.; Chung, J. W.; Seo, S.; Koo, B.; Kim, J. A Molecular Design Principle of Lyotropic Liquid-Crystalline Conjugated Polymers with Directed Alignment Capability for Plastic Electronics. *Nat. Mater.* **2013**, *12* (7), 659–664.
- (52) Giri, G.; Delongchamp, D. M.; Reinschamp, J.; Fischer, D. A.; Richter, L. J.; Xu, J.; Benight, S.; Ayzner, A.; He, M.; Fang, L.; et al. Effect of Solution Shearing Method on Packing and Disorder of

Organic Semiconductor Polymers. *Chem. Mater.* **2015**, *27* (7), 2350–2359.

(53) Shaw, L.; Hayoz, P.; Diao, Y.; Reinspach, J. A.; To, J. W. F.; Toney, M. F.; Weitz, R. T.; Bao, Z. Direct Uniaxial Alignment of a Donor–Acceptor Semiconducting Polymer Using Single-Step Solution Shearing. *ACS Appl. Mater. Interfaces* **2016**, *8* (14), 9285–9296.

(54) Shin, J.; Hong, T. R.; Lee, T. W.; Kim, A.; Kim, Y. H.; Cho, M. J.; Choi, D. H. Template-Guided Solution-Shearing Method for Enhanced Charge Carrier Mobility in Diketopyrrolopyrrole-Based Polymer Field-Effect Transistors. *Adv. Mater.* **2014**, *26* (34), 6031–6035.

(55) Khim, D.; Han, H.; Baeg, K. J.; Kim, J.; Kwak, S. W.; Kim, D. Y.; Noh, Y. Y. Simple Bar-Coating Process for Large-Area, High-Performance Organic Field-Effect Transistors and Ambipolar Complementary Integrated Circuits. *Adv. Mater.* **2013**, *25* (31), 4302–4308.

(56) Chang, M.; Choi, D.; Wang, G.; Kleinhenz, N.; Persson, N.; Park, B.; Reichmanis, E. Photoinduced Anisotropic Assembly of Conjugated Polymers in Insulating Polymer Blends. *ACS Appl. Mater. Interfaces* **2015**, *7* (25), 14095–14103.

(57) Chang, M.; Su, Z.; Egap, E. Alignment and Charge Transport of One-Dimensional Conjugated Polymer Nanowires in Insulating Polymer Blends. *Macromolecules* **2016**, *49* (24), 9449–9456.

(58) Schott, S.; Gann, E.; Thomsen, L.; Jung, S.-H.; Lee, J.-K.; McNeill, C. R.; Sirringhaus, H. Charge-Transport Anisotropy in a Uniaxially Aligned Diketopyrrolopyrrole-Based Copolymer. *Adv. Mater.* **2015**, *27* (45), 7356–7364.

(59) Lee, J.; Han, A.-R.; Kim, J.; Kim, Y.; Oh, J. H.; Yang, C. Solution-Processable Ambipolar Diketopyrrolopyrrole–Selenophene Polymer with Unprecedentedly High Hole and Electron Mobilities. *J. Am. Chem. Soc.* **2012**, *134* (51), 20713–20721.

(60) Back, J. Y.; Yu, H.; Song, I.; Kang, I.; Ahn, H.; Shin, T. J.; Kwon, S.-K.; Oh, J. H.; Kim, Y.-H. Investigation of Structure–Property Relationships in Diketopyrrolopyrrole-Based Polymer Semiconductors via Side-Chain Engineering. *Chem. Mater.* **2015**, *27* (5), 1732–1739.